



# Controlling Electrodeposition in Nonplanar High Areal Capacity **Battery Anodes via Charge Transport and Chemical Modulation**

Tian Tang, J. X. Kent Zheng, and Lynden A. Archer\*



Cite This: https://doi.org/10.1021/jacsau.3c00721



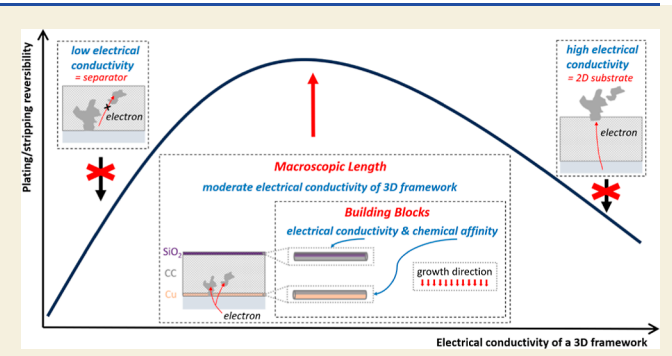
ACCESS I

Metrics & More

Article Recommendations

Supporting Information

ABSTRACT: Controlling the morphological evolution of electrochemical crystal growth in battery anodes is of fundamental and practical importance, particularly towards realizing practical, highenergy batteries based on metal electrodes. Such batteries require highly reversible plating/stripping reactions at the anode to achieve a long cycle life. While conformal electrodeposition and electrode reversibility have been demonstrated in numerous proof-of-concept experiments featuring moderate to low areal capacity (≤3 mA h/ cm<sup>2</sup>) electrodes, achieving high levels of reversibility is progressively challenging at the higher capacities (e.g., 10 mA h/ cm<sup>2</sup>), required in applications. Nonplanar, "3D" electrodes composed of electrically conductive, porous substrates are



conventionally thought to overcome trade-offs between reversibility and capacity because they hypothetically "host" the electrodeposits in an electronically conducting framework, providing redundant pathways for electron flow. Here, we challenge this hypothesis and instead show that a nonplanar substrate with moderate electrical conductivity (ideally, with an electrical conductance similar to the ionic conductance of the electrolyte) and composed of a passivated cathode-facing surface efficiently regulates electrocrystallization. In contrast, an architecture with a high intrinsic electrical conductivity or with a high electrical conductivity coating on the front surface results in dominantly out-of-plane growth, making the 3D architecture in effect function as a 2D substrate. Using Zn as an example, we demonstrate that interconnected carbon fiber substrates coated by SiO<sub>2</sub> on the front and Cu on the back successfully ushers electroplated Zn metal into the 3D framework at a macroscopic length scale, maximizing use of the interior space of the framework. The effective integration of electrodeposits into the 3D framework also enables unprecedented plating/stripping reversibility >99.5% at high current density (e.g., 10 mA/cm<sup>2</sup>) and high areal capacities (e.g., 10 mA h/cm<sup>2</sup>). Used in full-cell ZnII NaV<sub>3</sub>O<sub>8</sub> batteries with stringent N/P ratios of 3:1, the substrates are also shown to enhance cycle life.

KEYWORDS: batteries, metal anodes, electrodeposition, electrochemistry, charge transport, morphology, nonplanar architecture, surface chemistry

## MAIN TEXT BEGINS

Electrodes that harness plating/stripping reactions of pure metals are among the first explored in batteries historically, e.g., the Zn-Cu Daniel cell invented nearly 200 years ago. 12,13 Pure metallic electrodes have since been gradually, and now almost completely, replaced by those based on reversible intercalation/deintercalation of charge-carrying ions, with the most successful example being in rechargeable batteries, e.g., Li-ion cells. Compared with intercalation-type electrodes, electrodes relying on metal plating/stripping reactions continue to be of interest because of their higher specific capacity, versatility (e.g., the cathode need not be the source of electrochemically active metal ions), and in some cases lower cost. A significant body of work shows, however, that electrodes that rely on plating/stripping reactions are intrinsically unstable over the repeated cycles of growth and dissolution of metals therein required to sustain rechargeable battery operation. 4 Among the various failure mechanisms reported, the emerging

consensus is that processes (chemical, physical, mechanical) that deplete the active anode material are the most pernicious and difficult to eliminate. 15-19

Various approaches have nonetheless been reported that improve charge-discharge reversibility and cycle life of metal electrodes (e.g., via engineering the electrolyte, 20,21 separator,<sup>22</sup> electrode substrate,<sup>23</sup> and other components<sup>24</sup> of a battery electrode). Additionally, focused efforts to optimize one or more of these electrode/battery cell design features, has yielded steady improvements in reversibility of metal plating/ stripping reactions, which in the case of Li metal anodes can

November 17, 2023 Received: Revised: January 5, 2024 Accepted: January 8, 2024



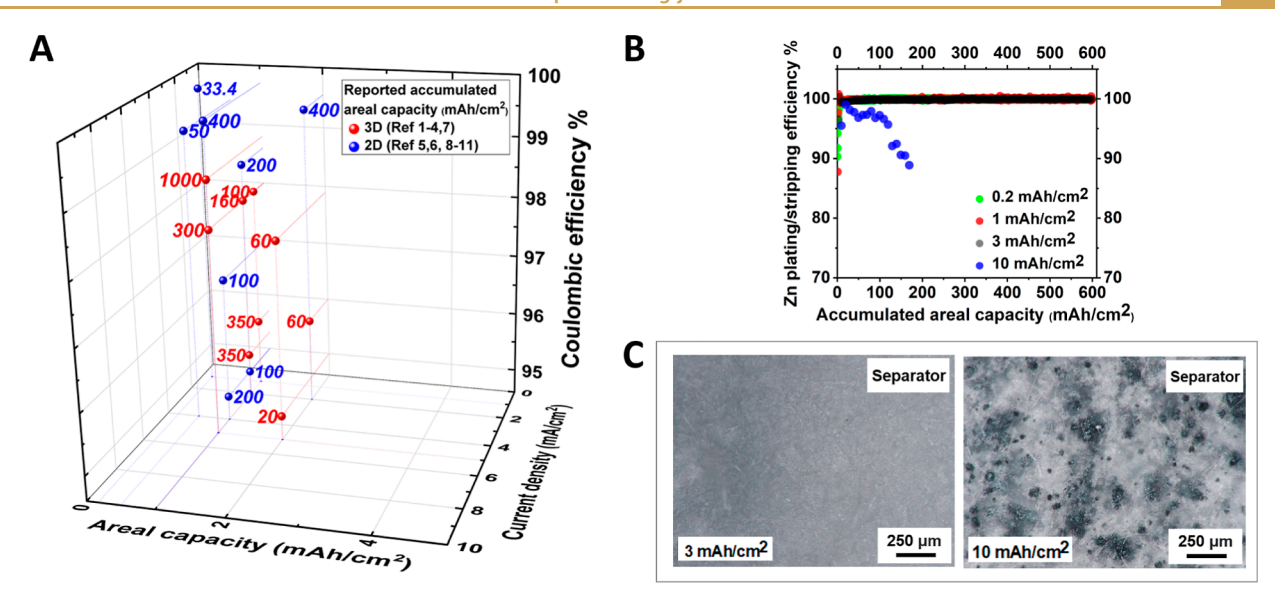


Figure 1. Critical areal capacity for metal plating/stripping processes in a battery anode. Progressively poorer reversibility is observed once the areal capacity of the electrode exceeds a certain critical value. (A) Summary of CE versus areal capacity values determined from state-of-the-art plating/stripping measurements reported in the contemporary literature.<sup>1–11</sup> The numbers represent the reported accumulated capacity over cycling (= areal capacity × cycle number). The areal capacities used are consistently below 2 mA h/cm². (B) Evaluation of plating/stripping reversibility of Zn at different areal capacities. The measurements all use Cu foil, a substrate known to alloy with Zn to promote high Zn reversibility, as a current collector. A critical areal capacity of 3 mA h/cm² is observed, above which the cell suffers from rapid failure. (C) Optical microscopy images of the separator facing the Cu substrate after Zn plating/stripping, at 3 mA h/cm², and at 10 mA h/cm², respectively.

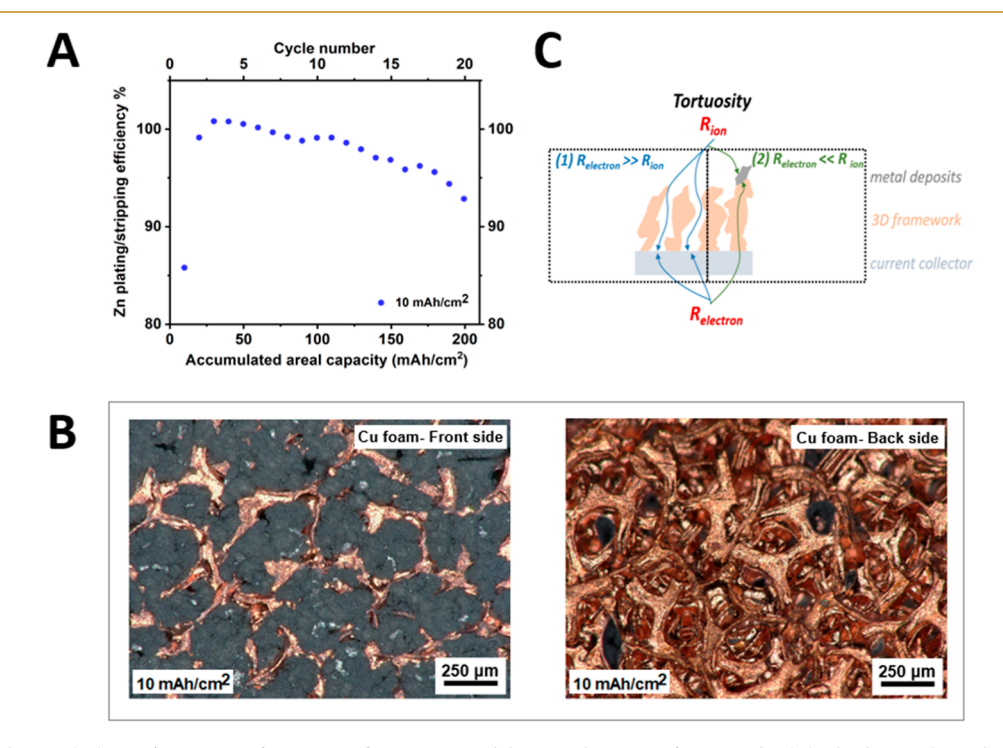


Figure 2. Electrochemical plating/stripping of Zn in Cu foam as a model 3D architecture featuring both high electrical conductivity and chemical affinity. (A) Zn plating/stripping CE at  $10 \text{ mA h/cm}^2$ . (B) Optical microscopy images of Cu foam facing the separator (left), and facing the current collector on the back (right). Zn preferentially grows only on the top surface of 3D Cu foam, making the architecture a 2D substrate in effect. (C) Analysis of transport of charged species and the resulting electrodeposition morphology in the 3D architecture.

achieve Coulombic efficiency (CE) values close-to-unity, i.e., >99%. These promising developments have collectively contributed to a contemporary revival in scientific and technological interest for electrodes utilizing plating/stripping reactions.

With few exceptions<sup>26,27</sup> in systems such as Li—a relatively soft material with a low modulus—the high levels of plating/

stripping reversibility required for practical battery applications (e.g., CE > 99%), are reported in experiments based on electrochemical cells with low (<2 mA h/cm²) or at best moderate ( $\sim$ 3 mA h/cm²) areal capacity electrodes. This situation contrasts with the typically high areal capacities ( $\sim$ 10 mA h/cm²) required for commercial battery cells to provide the cell-level energy densities demanded by even the least

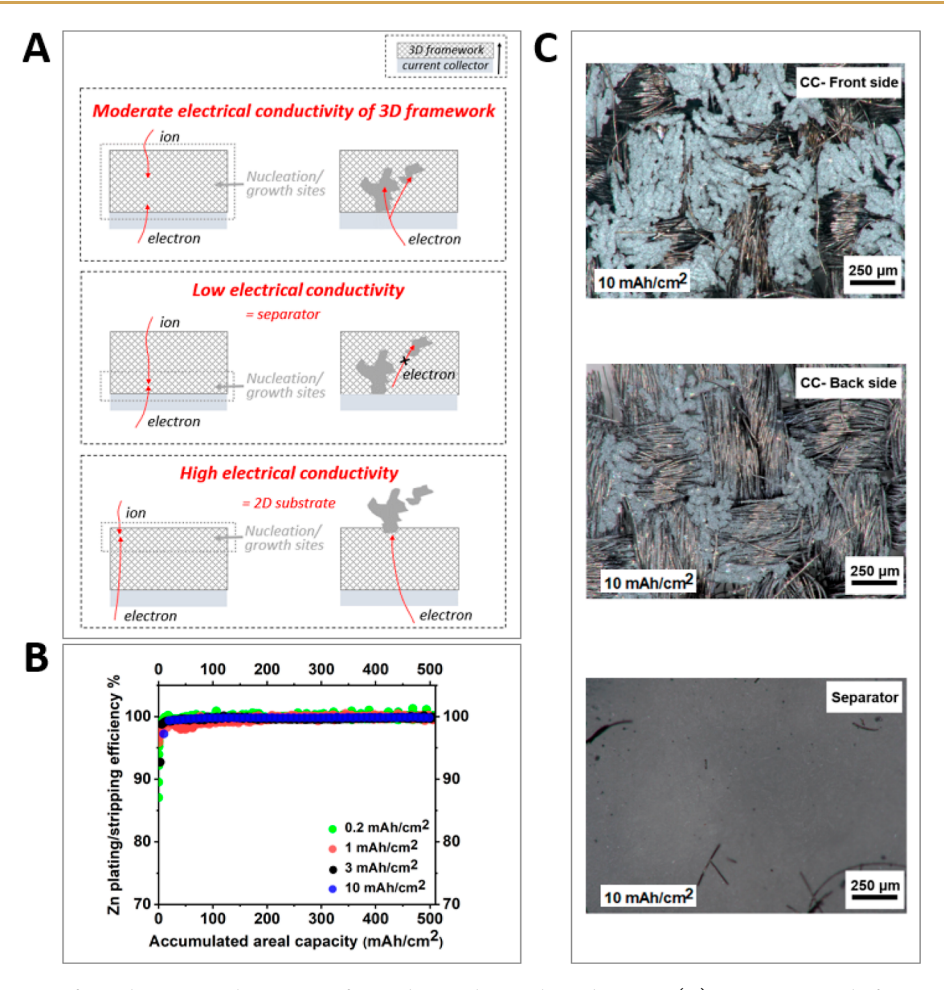


Figure 3. Electrodeposition of metals in 3D architectures of a moderate electrical conductivity. (A) Design principle for 3D architectures based on electrical conductivity. (B) Zn plating/stripping Coulombic efficiencies at different areal capacities on carbon-cloth electrodes, an architecture with moderate electrical conductivity. (C) Optical microscopy images of Zn growth on the front and the backside of the carbon cloth architecture after plating, and of the separator facing the electrode after stripping ( $10 \text{ mA h/cm}^2$ ). The black fibers on separator are debris of the carbon cloth produced in cell disassembling.

demanding applications in transportation. We illustrate this challenge in Figure 1A using results from contemporary, stateof-the-art experimental results in the literature employing battery cells based on Zn anodes in mild-to-neutral pH electrolytes. 1–11 The summary in Figure 1B focuses on electrodes based on Cu foil as a current collector; a substrate known to be electrochemically inert in mild aqueous electrolytes used for Zn batteries and also to enable high plating/stripping reversibility over extended cycling by regulating crystallization of the Zn deposits.<sup>28–30</sup> The results are consistent with a common understanding: there is evidently a trade-off between areal capacity and plating/ stripping reversibility. As shown in Figure 1B and Figures S1-2, the Zn plating/stripping process on Cu is stable when the areal capacity is kept below 3 mA h/cm<sup>2</sup> but is significantly destabilized as the areal capacity approaches 10 mA h/cm<sup>2</sup>. Post-mortem optical-microscopy analyses in Figure 1C of the cell cycled at 10 mA h/cm<sup>2</sup> show that Zn electrodeposits penetrate into the glass fiber separator and are likely electrochemically "orphaned" due to the breakdown of electronic wiring in dissolution. This can be contrasted with the corresponding optical micrographs obtained under lowareal-capacity conditions, where the separator remains essentially Zn free! Our observations suggest that even under conditions where the electrodeposition is effectively regulated

at the surface of a planar Cu substrate, the desired compact growth mode is eventually lost at higher areal capacity. Growth of the metal deposits instead transforms into what we term an "aggressive" mode that eventually ends in electrode/cell failure when the areal capacity exceeds a certain critical value,  $Q_c$ , which according to the measurements in Figure 1B is approximately 3 mA h/cm² for deposition of Zn on a planar, 2D Cu substrate.

Electrode failure at high areal capacities has been conventionally argued to correlate with transport limitations and intrinsic electrokinetics of an electrolyte as determined by the sand's capacity. 31,32 This would imply that the onset condition is independent of the heterointerfacial interactions at the surface of a 2D substrate.<sup>21</sup> Hosting electrodeposits in an electrically conductive 3D architecture simultaneously provides a straightforward test of this hypothesis and potentially offers an avenue toward achieving higher  $Q_c$ . In theory, high reversibility at elevated capacities is anticipated for 3D architecture because they supply robust electronic pathways for the large number of metal deposits produced in charging. The pores inside a 3D architecture also facilitate the storage of more deposits, while maintaining electrical connectivity and hence electrochemical activity of the deposits. Surprisingly, experimental measurements of Zn plating/stripping on a 3D Cu foams selected as a model system, 7,33 indicate that the 3D

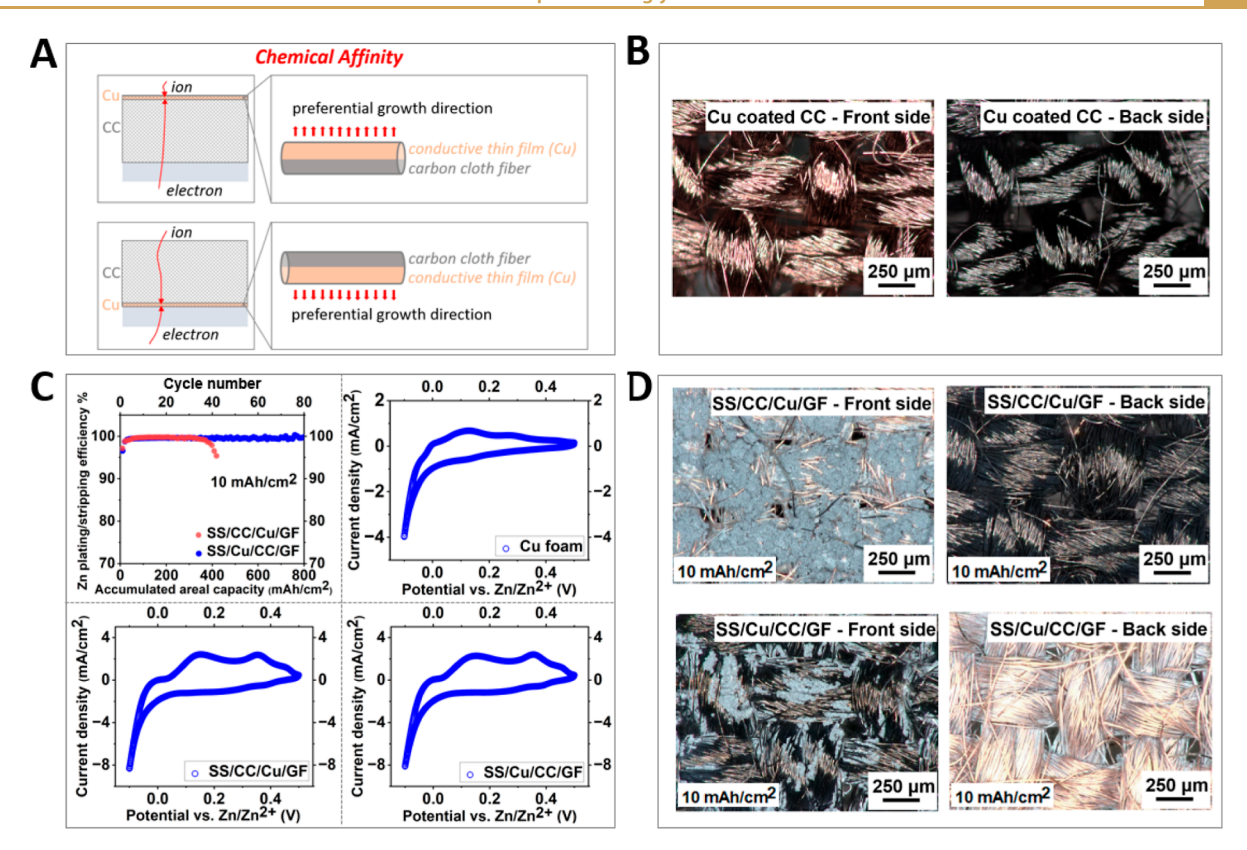


Figure 4. Tailoring chemical affinity of the building-block structure in a 3D architecture. (A) Design principle of chemical affinity for 3D architectures. (B) Optical microscopy images of a Cu-coated carbon architecture. (C) Electrochemical analyses of Zn plating/stripping on Cu-coated carbon architectures. (D) Optical microscopy images of Zn electrodeposition on Cu-coated carbon architecture.

electrode architecture introduces minimal—if any at all—improvement in reversibility at 10 mA h/cm<sup>2</sup>, and cycling ends in fast failure after only 10 charge—discharge cycles (Figure 2A and Figure S3 for voltage profile).

The findings for Zn plating/stripping on Cu foam are the more surprising given the well-known high electrical conductivity (resistivity  $\rho=1.8\times10^{-6}~\Omega\cdot\text{cm}$ ) and inertness of Cu under the conditions of the experiments. A more reasonable expectation would be for the Cu foam to provide multiple, redundant pathways of electronically accessing Zn deposits—even deposits that might be considered orphaned at a 2D Cu electrode—increasing electrode reversibility and battery cell cycle life. Moreover, Cu has been reported in multiple prior studies, including ours. To alloy with Zn, which would strongly anchor the Zn deposits to minimize their mechanical disconnection and orphaning.

We analyzed the micrometer scale structure of Zn electrodeposited on 3D Cu foams using optical microscopy. Results reported in Figure 2B show that the Zn electrodeposits predominantly exist on the counter electrode-facing, "front" side of the Cu foam; no Zn deposits are discernible on the backside thereof. See also low-magnification optical microsocpy images in Figure S4. After nucleation on the front surface of the Cu foam, the Zn electrodeposit growth is dominantly normal to the substrate and toward the glass fiber separator. This means that the geometrically-3D Cu foam in effect functions as a 2D substrate because only the front surface is in contact with Zn metal deposits. The inner pores of the 3D framework—which presumably should have hosted the bulk of the electrodeposits— in contrast remain zinc-free, clean, and therefore inactive. The results suggest that even a

nominally 3D current collector does not necessarily promote the 3D electrocrystallization of metal ions deposited from an electrolyte. It is then of fundamental interest to understand the factors that regulate the spatial distribution of electrochemically grown metals in a 3D electronically conductive framework. Such an understanding would in turn provide key design rules for creating 3D electrodes that fully utilize the inner space of the electrode to stabilize metal plating/stripping at high areal capacities.

Coupled charge transport in electron- and ion-conducting phases of a battery electrode are understood to play complementary yet distinct roles in the nucleation and growth of electrodeposited metals in essentially any electrode, whether 2D or 3D.  $^{14,35,36}$  The characteristic relaxation time  $\tau$  of a diffusional process is proportional to the square of diffusion length L over diffusivity D (i.e.,  $\tau \sim {^L^2}\!/_D$ ). Diffusivity is related to the resistivity of a material by the Einstein relation, taking into account the charge carrier concentration. As illustrated in Figure 2C, considering the charge transport mechanisms where the metal electrodeposits nucleate at the front and the back surfaces of a 3D current collector substrate, respectively, fast transport of electrons is evidently associated with preferential growth on the front-facing side of the current collector. This holds true if  $R_e \ll R_{ion}$ , for example, when the 3D framework is made of an excellent electron conductor such as Cu. At the other extreme, i.e.,  $R_e \gg R_{ion}$ , the nucleation predominantly occurs on the back surface of the 3D framework; a piece of glass-fiber filter exemplifies such a 3D framework. While this scenario appears to be capable of promoting electrodeposit growth inside the 3D framework, it is of course not ideal because a current collector framework with its low electrical

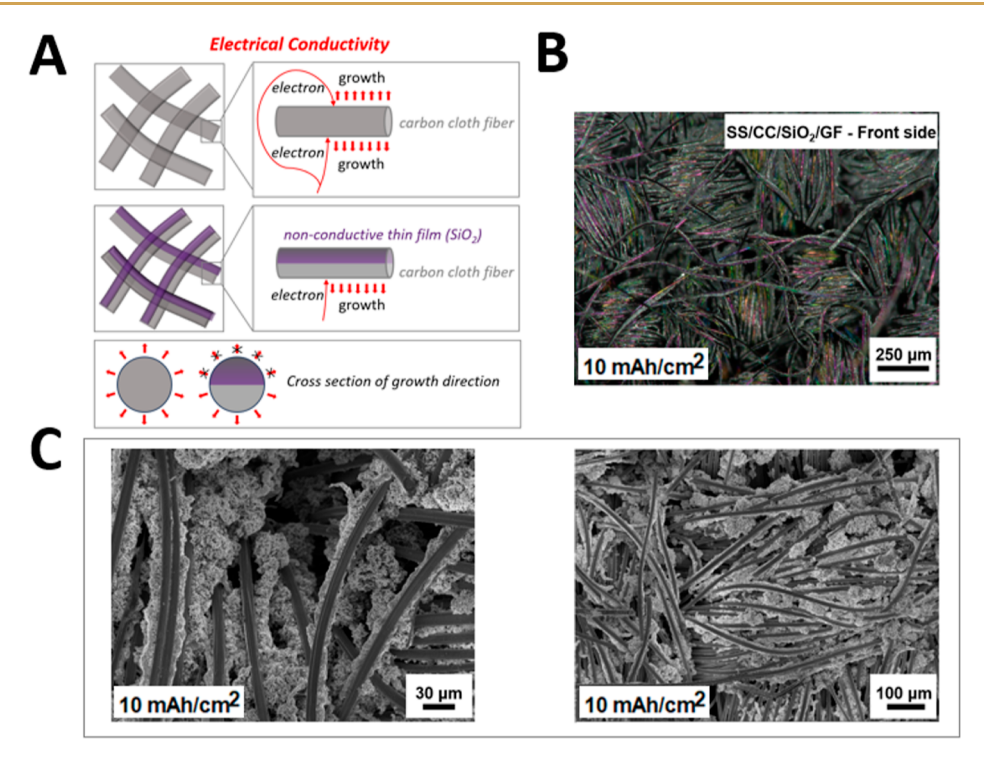


Figure 5. Tuning electrical conductivity of the building-block structure in a 3D architecture. (A) Design principle for electrical conductivity at the individual fiber level. (B) Optical microscopy and (C) scanning electron microscopy images of Zn electrodeposition on SiO<sub>2</sub>-coated carbon fibers.

conductivity would no longer be capable of serving the original purpose of supplying robust electronic wiring to the metal deposits.

Considerations of the coupled charge transport at the electrochemical interface imply that a 3D framework made of a material with moderate electrical conductivity could provide an interesting balance between the resistances originating from electronic and ionic transport (Figure 3A), which would in turn favor full and reversible utilization of the interior space of a 3D current collector. It would promote nucleation and growth of metal inside the 3D framework while maintaining the electronic wiring. Motivated by this hypothesis, we choose a framework made of carbon fibers with  $\rho = 1.1 \times 10^{-3} \ \Omega \cdot \text{cm}$ , 3 orders of magnitude higher than Cu, but still much lower than  $SiO_2$  ( $\rho > 10^{14} \Omega \cdot cm$ ). Electrical measurements reported in Figure S5 show that the resistance of the 3D carbon-based substrate is on the order or 1  $\Omega$ , whereas it is ~0.01  $\Omega$  for Cu. To estimate the ionic resistance of the electrolyte, we measured the uncompensated Ohmic resistance  $R_{ij}$  of a Znll Zn symmetric cell using electrochemical impedance spectroscopy;<sup>37</sup> Given that the electrical resistance of the metal parts is on the order of 0.01  $\Omega$ , we attribute the measured  $R_u$  of  $\sim 2 \Omega$ primarily to the ionic resistance of the electrolyte. The measured values are interestingly comparable to the electrical resistance of the carbon electrode, confirming that for the carbon architecture, the electrolyte, and the framework conductances are of comparable order of magnitude.

Zn plating/stripping tests performed on the carbon fiber frameworks at areal capacities from 0.2 to 10 mA h/cm² show excellent reversibility and stability (see CE values in Figure 3B and Figures S6~7). The instability associated with Zn plating/stripping at high areal capacities (e.g., 10 mA h/cm²) is also shown to be effectively suppressed on a 3D carbon architecture, as evidenced by the high CE and cycling performance observed. More straightforward is that Zn

electrodeposits can be seen from both the back surface and the front surface of the current collector (Figure 3C), suggesting a more uniform distribution of the Zn and improved spatial utilization within the 3D framework. The separator here also remains clean and no dead zinc is observed.

Electrodeposition of Zn in the 3D carbon framework therefore unambiguously elucidates the role of the coupled transport of ions and electrons in controlling the spatial distribution of metal electrodeposits. On the one hand, it offers perspective about the factors responsible for the trade-off between electrode reversibility and areal capacity at high areal capacities —i.e., conduction of charged species— and offers insights about how the electrochemical growth of metals in complex current collector architectures might be controlled. On the other hand, our findings raise questions about conventional design rules based on the idea that chemical affinity/metal-philicity/and alloying of the deposited metal to a 3D substrate regulate where the electrochemical nucleation and growth happen in a 3D substrate (Figures S8—9).

To study the influence of the first of these features, chemical modulation, we alternately coated the front side (facing the separator and counter-electrode) and backside (facing the current collector) of a 3D carbon framework with a few layers of Cu (Figure 4A). The Cu deposition is performed by means of high-vacuum magnetron sputtering that creates uniform, complete coverage of the framework at the individual fiber level but only on one side of the framework facing the source material (Figure 4B and Figure S10). As discussed earlier, Cu has been shown in several studies to alloy with the electrodeposited Zn and allows extremely stable plating/ stripping on 2D substrates when the areal capacity is small. Notable differences are observed in Zn plating/stripping on the Cu-coated carbon framework. The plating/stripping on the carbon framework with Cu on the back, for example, manifests a significantly longer cycle life with close-to-unity reversibility

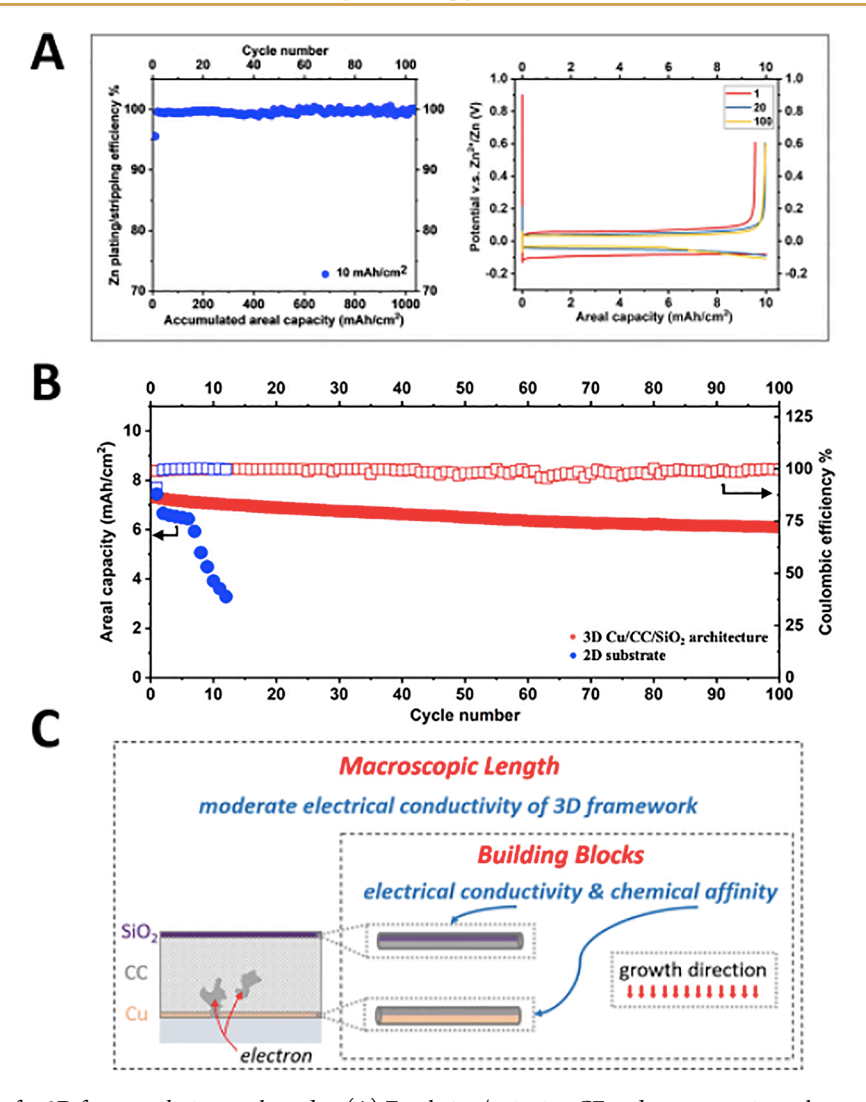


Figure 6. Design principles for 3D frameworks in metal anodes. (A) Zn plating/stripping CE and representative voltage profile. The numbers in the legends denote the cycle number. (B) Full cell demonstration using Zn||NaV $_3$ O $_8$ , with an N/P ratio or 3:1, at an areal capacity of  $\sim$ 8 mA h/cm $^2$ . (C) Illustration of the design principles.

at 10 mA h/cm<sup>2</sup> (Figure 4C), whereas the carbon framework with Cu on the front fails after only 40 cycles. The voltage features specific to Zn-Cu alloying are observed in the voltage profiles of both samples (Figure S11). This is consistent with the cyclic voltammetry measurements that confirm the presence of Zn-Cu alloying reactions in both cases; a minimal difference between the two samples is observed in CV. The similar current densities observed on SS/CC/Cu/GF and SS/ Cu/CC/GF, respectively, indicate that the PVD-deposited Cu layer is effectively guiding Zn deposition regardless of whether it is facing forward (i.e., separator) or backward (i.e., SS current collector). The higher current densities on these two PVD-deposited Cu than commercial Cu foam could result from the fact that PVD-deposited Cu is oftentimes enriched by defects and nanoscale boundaries,<sup>38</sup> which allows faster reaction kinetics. Microscopy characterization results corroborate these analyses; It is found that Zn preferentially grows on the front side of a front-Cu-coated carbon framework toward the separator, leaving the inside and the backside clean. For the back-Cu-coated carbon framework, uniform Zn nucleation and conformal growth at the fiber level are seen on the backside of the carbon framework, which subsequently leads to Zn deposits mostly embedded among the fibers when viewed

from the front side. Such morphological dissimilarities, in a well-expected manner, give rise to the observed electrochemical behaviors. The uniform distribution of Zn deposited into the nonplanar current collector guarantees effective electronic wiring in the dissolution process. In contrast, for current collectors that promote nonuniform Zn growth on the surface, the dissolution is observed to involve significant orphaning due to the fragility of electronic conduction paths inherent to aggressive growth patterns. The difference in morphological evolution eventually results in different plating/stripping reversibility.

The spatial distribution of Zn on the two types of Cu-coated carbon frameworks can be understood by accounting for both the charge transport and chemical modulation. When Cu is present on the front surface of the carbon framework, Cu not only chemically induces Zn to nucleate thereupon but also increases the electrical conductivity on the front surface. The subsequent Zn growth favors an outward direction into the separator (Figure 4D). By contrast, the Cu on the back-coated carbon framework facilitates nucleation of Zn at the backside of the framework and ensures the subsequently grown Zn structures' effective hosting by the 3D framework. This means that a metal-philic layer beneath a 3D framework promotes

nucleation at the bottom and the metal extends into the 3D framework in the growth stage.

Inspired by the capability of magnetron sputtering to prepare coating with high precision on the individual fiber level as demonstrated by the Cu case, we use this method to prepare 3D carbon frameworks with SiO<sub>2</sub> coatings—which are highly electrically insulative,<sup>37</sup> on the contrary to the Cu coatings explored in the previous case—on the front side facing the counter electrode; see an illustration in Figure 5A. (See also Table S1 for compositional analysis). The design is intended to electrically passivate the front side of the fibers, minimize nucleation and growth outward, and eventually guide preferential growth of the metal inside the 3D framework. Microscopy results unambiguously show that the growth selectively happens on the back side of individual fibers (Figure 5B,C), and therefore, they validate such an approach based on charge transport modulation. Consequently, improved Zn plating-stripping reversibility is observed (Figure S12). When coupled with a Cu-enriched layer facing the current collector, the electrode Cu/CC/SiO<sub>2</sub> shows a even higher, more stable Zn plating/stripping behavior (Figure 6A). We further evaluated this concept in a practical full-battery setup (Figure 6B and Figure S13). The full battery consisting of a Zn anode and a sodium vanadate cathode<sup>39-41</sup> shows stable charge discharge performance at a high areal capacity of 8 mA h/cm<sup>2</sup> over prolonged cycling. Of particular note is that a limited amount of Zn is predeposited onto the Cu/CC/SiO<sub>2</sub> architecture to ensure a practical N/P ratio of 3:1.

Taken together, our findings show that a 3D framework with moderate electrical conductivity, a front surface passivated by an insulator, and a back surface functionalized by a metal-philic layer would represent the ideal design for guaranteeing utilization of the inner pore of a 3D architecture (Figure 6C). 3D frameworks that satisfy these design requirements hold the potential for achieving high metal plating/stripping reversibility and stable cycling of full batteries at high areal capacities. The results open up new opportunities for electrode designs that regulate where electro-crystallization of metals occur in an electrode. In so doing, they provide a simple, scalable approach for overcoming trade-offs between electrode reversibility and areal capacity, enabling progress toward commercially relevant metal electrodes with high areal capacities.

## **■ EXPERIMENTAL SECTION**

#### **Materials**

Zn foil (99.9%), ZnSO<sub>4</sub>·7H<sub>2</sub>O (99.95%), V<sub>2</sub>O<sub>5</sub> (99.95%), and poly(vinylidene fluoride) were purchased from Sigma-Aldrich. Cu foil (99.8%; 0.025 mm) and Cu foam were purchased from MTI. Plain carbon cloth 1071 was purchased from Fuel Cell Store. Ketjen black carbon was purchased from AkzoNobel. Plain carbon cloth was coated with Cu and SiO<sub>2</sub> by a magnetron argon sputtering deposition system with a setting thickness of 500 nm. Deionized water was obtained from Milli-Q water purification system. Zn electrolytes were prepared by dissolving ZnSO<sub>4</sub>·7H<sub>2</sub>O in deionized water (2 M). Whatman glass microfiber filter grade GF/A was used as the separator. NVO cathode material was synthesized according to the approach reported in a previous study. <sup>42</sup> The weight ratio of the cathode between NVO, ketjen black, and polyvinylidene fluoride was 80:10:10. The cathode was later dispersed into carbon cloth as stated by our prior study. <sup>43</sup>

#### **Characterization of Materials**

Scanning electron microscopy was carried out on a Zeiss Gemini 500 Scanning Electron Microscope. Measurements were collected using the Thermo Scientific Nexsa G2 X-ray photoelectron spectrometer with the survey spectrum and high sensitivity spectra collected at 200 eV pass energy and the high-resolution scans collected at 50 eV. Optical microscopy was performed on a Keyence VHX microscope.

## **Electrochemical Measurements**

Galvanostatic charge/discharge performance of coin cells were tested on Neware battery test systems at room temperature. Cyclic voltammetry tests were performed on a CH instrument electrochemical workstation with a scan rate of 20 mv/s. Electrochemical impedance spectroscopy was performed on a Biologic SP-200 potentiometer. Electrochemical studies were performed by using CR2032 coin cells. The area of electrodes in this study is 0.71 cm<sup>2</sup>. Electrodes are separated by glass fiber.  $\sim 100 \ \mu L$  of electrolyte is added into each cell using a pipet. Current density is 10 mA/cm<sup>2</sup> unless specified. In a zinc plating/stripping CE measurement (using a ZnllCu cell), zinc metal is plated on the substrate with a known current and capacity, and then the metal deposit is stripped with the reverse current until the electrochemical potential reaches a threshold. The CE (plating/stripping efficiency) quantifies the reversibility of the metal plating/stripping process on the substrate of interest and is calculated according to

Coulombic efficiency = 
$$\frac{\text{stripping capacity}}{\text{plating capacity}} \times 100\%$$

## ASSOCIATED CONTENT

## Supporting Information

The Supporting Information is available free of charge at https://pubs.acs.org/doi/10.1021/jacsau.3c00721.

Electrochemical, chemical, electrical, and microscopy characterization data (PDF)

## AUTHOR INFORMATION

#### **Corresponding Author**

Lynden A. Archer — Robert Frederick Smith School of Chemical and Biomolecular Engineering, Cornell University, Ithaca, New York 14853, United States; orcid.org/0000-0001-9032-2772; Email: laa25@cornell.edu

## Authors

Tian Tang – Department of Materials Science and Engineering, Cornell University, Ithaca, New York 14853, United States

J. X. Kent Zheng – McKetta Department of Chemical Engineering, The University of Texas at Austin, Austin, Texas 78712, United States

Complete contact information is available at: https://pubs.acs.org/10.1021/jacsau.3c00721

## **Author Contributions**

L.A.A. directed this project. T.T., J.X.K.Z., and L.A.A. conceived and designed this work. T.T. performed experiments and characterizations. All the authors analyzed and discussed the data. T.T. and L.A.A. wrote the manuscript with important input from all the authors.

#### Notes

The authors declare no competing financial interest.

## ACKNOWLEDGMENTS

Funding: This work was supported as part of the Center for Mesoscale Transport Properties, an Energy Frontier Research Center supported by the U.S. Department of Energy, Office of Science, Basic Energy Sciences, under award #DE-SC0012673. The work made use of the Cornell Center for Materials Research Shared Facilities, which are supported through the NSF MRSEC program (DMR-1719875).

## REFERENCES

- (1) Zeng, Y.; Zhang, X.; Qin, R.; Liu, X.; Fang, P.; Zheng, D.; Tong, Y.; Lu, X. Dendrite-free zinc deposition induced by multifunctional CNT frameworks for stable flexible Zn-ion batteries. *Adv. Mater.* **2019**, *31* (36), 1903675.
- (2) Zeng, Y.; Sun, P. X.; Pei, Z.; Jin, Q.; Zhang, X.; Yu, L.; Lou, X. W. Nitrogen-doped carbon fibers embedded with zincophilic Cu nanoboxes for stable Zn-metal anodes. *Adv. Mater.* **2022**, *34* (18), 2200342.
- (3) An, Y.; Tian, Y.; Li, Y.; Wei, C.; Tao, Y.; Liu, Y.; Xi, B.; Xiong, S.; Feng, J.; Qian, Y. Heteroatom-doped 3D porous carbon architectures for highly stable aqueous zinc metal batteries and non-aqueous lithium metal batteries. *Chem. Eng. J.* **2020**, *400*, 125843.
- (4) Cao, Q.; Gao, H.; Gao, Y.; Yang, J.; Li, C.; Pu, J.; Du, J.; Yang, J.; Cai, D.; Pan, Z.; et al. Regulating dendrite-free zinc deposition by 3D zincopilic nitrogen-doped vertical graphene for high-performance flexible Zn-ion batteries. *Adv. Funct. Mater.* **2021**, *31* (37), 2103922.
- (5) Fu, J.; Guo, Y.; Wang, H.; Xiao, P.; Liang, J.; Sun, Q.; Li, H. Circumventing the zinc dendrites via contact-actuated aspectant growth. *Energy Storage Mater.* **2023**, *61*, 102856.
- (6) Hao, J.; Li, X.; Zhang, S.; Yang, F.; Zeng, X.; Zhang, S.; Bo, G.; Wang, C.; Guo, Z. Designing dendrite-free zinc anodes for advanced aqueous zinc batteries. *Adv. Funct. Mater.* **2020**, *30* (30), 2001263.
- (7) Shi, X.; Xu, G.; Liang, S.; Li, C.; Guo, S.; Xie, X.; Ma, X.; Zhou, J. Homogeneous deposition of zinc on three-dimensional porous copper foam as a superior zinc metal anode. *ACS Sustainable Chem. Eng.* **2019**, 7 (21), 17737–17746.
- (8) Wang, F.; Borodin, O.; Gao, T.; Fan, X.; Sun, W.; Han, F.; Faraone, A.; Dura, J. A.; Xu, K.; Wang, C. Highly reversible zinc metal anode for aqueous batteries. *Nat. Mater.* **2018**, *17* (6), 543–549.
- (9) Wang, N.; Chen, X.; Wan, H.; Zhang, B.; Guan, K.; Yao, J.; Ji, J.; Li, J.; Gan, Y.; Lv, L.; et al. Zincophobic Electrolyte Achieves Highly Reversible Zinc-Ion Batteries. *Adv. Funct. Mater.* **2023**, 33, 2300795.
- (10) Xiao, P.; Wu, Y.; Fu, J.; Liang, J.; Zhao, Y.; Ma, Y.; Zhai, T.; Li, H. Enabling high-rate and high-areal-capacity Zn deposition via an interfacial preferentially adsorbed molecular layer. *ACS Energy Lett.* **2023**, 8 (1), 31–39.
- (11) Xie, F.; Li, H.; Wang, X.; Zhi, X.; Chao, D.; Davey, K.; Qiao, S. Z. Mechanism for zincophilic sites on zinc-metal anode hosts in aqueous batteries. *Adv. Energy Mater.* **2021**, *11* (9), 2003419.
- (12) Volta, A., XVII. On the electricity excited by the mere contact of conducting substances of different kinds. In a letter from Mr. Alexander Volta, FRS Professor of Natural Philosophy in the University of Pavia, to the Rt. Hon. Sir Joseph Banks, Bart. KBPR S. Phil. Trans. Roy. Soc. Lond. 1832, 1 (90), 403–431.
- (13) Daniell, J. F. X. On Voltaic Combinations. In a letter addressed to Michael Faraday, DCL, FRS, Fullerian Prof. Chem. Royal Institution, Corr. Memb. Royal & Imp. Acadd. of Science, Paris, Petersburgh, &c. By J. Frederic Daniell, FRS, Prof. Chem. in King's College, London. *Philos. Trans. R. Soc. London* 1836, 3 (126), 107–124.
- (14) Zheng, J.; Garcia-Mendez, R.; Archer, L. A. Engineering Multiscale Coupled Electron/Ion Transport in Battery Electrodes. *ACS Nano* **2021**, *15* (12), 19014–19025.
- (15) Peled, E. The electrochemical behavior of alkali and alkaline earth metals in nonaqueous battery systems-the solid electrolyte interphase model. *J. Electrochem. Soc.* **1979**, *126* (12), 2047–2051.
- (16) Peled, E.; Menkin, S. Review—SEI: Past, Present and Future. *J. Electrochem. Soc.* **2017**, *164* (7), A1703–A1719.

- (17) Zheng, J.; Kim, M. S.; Tu, Z.; Choudhury, S.; Tang, T.; Archer, L. A. Regulating electrodeposition morphology of lithium: towards commercially relevant secondary Li metal batteries. *Chem. Soc. Rev.* **2020**, 49 (9), 2701–2750.
- (18) Zachman, M. J.; Tu, Z.; Choudhury, S.; Archer, L. A.; Kourkoutis, L. F. Cryo-STEM mapping of solid-liquid interfaces and dendrites in lithium-metal batteries. *Nature* **2018**, *560* (7718), 345–349.
- (19) Lin, D.; Liu, Y.; Cui, Y. Reviving the lithium metal anode for high-energy batteries. *Nat. Nanotechnol.* **2017**, *12* (3), 194–206.
- (20) Cao, L.; Li, D.; Hu, E.; Xu, J.; Deng, T.; Ma, L.; Wang, Y.; Yang, X.-Q.; Wang, C. Solvation structure design for aqueous Zn metal batteries. J. Am. Chem. Soc. 2020, 142 (51), 21404–21409.
- (21) Zhang, T.; Tang, Y.; Guo, S.; Cao, X.; Pan, A.; Fang, G.; Zhou, J.; Liang, S. Fundamentals and perspectives in developing zinc-ion battery electrolytes: a comprehensive review. *Energy Environ. Sci.* **2020**, *13* (12), 4625–4665.
- (22) Liang, J.; Chen, Q.; Liao, X.; Yao, P.; Zhu, B.; Lv, G.; Wang, X.; Chen, X.; Zhu, J. A nano-shield design for separators to resist dendrite formation in lithium-metal batteries. *Angew. Chem.* **2020**, *132* (16), 6623–6628.
- (23) Wei, X.; Desai, D.; Yadav, G. G.; Turney, D. E.; Couzis, A.; Banerjee, S. Impact of anode substrates on electrodeposited zinc over cycling in zinc-anode rechargeable alkaline batteries. *Electrochim. Acta* **2016**, *212*, 603–613.
- (24) Desai, D.; Wei, X.; Steingart, D. A.; Banerjee, S. Electro-deposition of preferentially oriented zinc for flow-assisted alkaline batteries. *J. Power Sources* **2014**, *256*, 145–152.
- (25) Zheng, J. X. K. Perspective-Reversibility of Electro-Plating/ Stripping Reactions: Metal Anodes for Rechargeable Batteries. *J. Electrochem. Soc.* **2022**, *169* (10), 100532.
- (26) Zheng, J.; Tang, T.; Zhao, Q.; Liu, X.; Deng, Y.; Archer, L. A. Physical orphaning versus chemical instability: is dendritic electrodeposition of Li fatal? *ACS Energy Lett.* **2019**, *4* (6), 1349–1355.
- (27) Zhao, Q.; Deng, Y.; Utomo, N. W.; Zheng, J.; Biswal, P.; Yin, J.; Archer, L. A. On the crystallography and reversibility of lithium electrodeposits at ultrahigh capacity. *Nat. Commun.* **2021**, *12* (1), 6034–6110.
- (28) Zheng, J.; Deng, Y.; Li, W.; Yin, J.; West, P. J.; Tang, T.; Tong, X.; Bock, D. C.; Jin, S.; Zhao, Q.; et al. Design principles for heterointerfacial alloying kinetics at metallic anodes in rechargeable batteries. *Sci. Adv.* **2022**, *8* (44), No. eabq6321.
- (29) Li, B.; Yang, K.; Ma, J.; Shi, P.; Chen, L.; Chen, C.; Hong, X.; Cheng, X.; Tang, M. C.; He, Y. B.; et al. Multicomponent copper-zinc alloy layer enabling ultra-stable zinc metal anode of aqueous Zn-ion battery. *Angew. Chem., Int. Ed.* **2022**, *61* (47), No. e202212587.
- (30) Yang, S.; Li, Y.; Du, H.; Liu, Y.; Xiang, Y.; Xiong, L.; Wu, X.; Wu, X. Copper nanoparticle-modified carbon nanofiber for seeded zinc deposition enables stable Zn metal anode. ACS Sustainable Chem. Eng. 2022, 10 (38), 12630–12641.
- (31) Zheng, J.; Yin, J.; Zhang, D.; Li, G.; Bock, D. C.; Tang, T.; Zhao, Q.; Liu, X.; Warren, A.; Deng, Y.; et al. Spontaneous and field-induced crystallographic reorientation of metal electrodeposits at battery anodes. *Sci. Adv.* **2020**, *6* (25), No. eabb1122.
- (32) Bai, P.; Li, J.; Brushett, F. R.; Bazant, M. Z. Transition of lithium growth mechanisms in liquid electrolytes. *Energy Environ. Sci.* **2016**, 9 (10), 3221–3229.
- (33) Li, C.; Shi, X.; Liang, S.; Ma, X.; Han, M.; Wu, X.; Zhou, J. Spatially homogeneous copper foam as surface dendrite-free host for zinc metal anode. *Chem. Eng. J.* **2020**, *379*, 122248.
- (34) Zheng, J.; Deng, Y.; Li, W.; Yin, J.; West, P. J.; Tang, T.; Tong, X.; Bock, D. C.; Jin, S.; Zhao, Q.; et al. Design Principles for Heterointerfacial Alloying Kinetics at Metallic Anodes in Rechargeable Batteries. *Sci. Adv.* **2022**, *8*, abq6321.
- (35) Zhang, X.; Ju, Z.; Zhu, Y.; Takeuchi, K. J.; Takeuchi, E. S.; Marschilok, A. C.; Yu, G. Multiscale Understanding and Architecture Design of High Energy/Power Lithium-Ion Battery Electrodes. *Adv. Energy Mater.* **2020**, *11*, 2000808.

- (36) Zhu, C.; Usiskin, R. E.; Yu, Y.; Maier, J. The nanoscale circuitry of battery electrodes. *Science* **2017**, 358 (6369), No. eaao2808.
- (37) Lazanas, A. C.; Prodromidis, M. I. Electrochemical Impedance Spectroscopy-A Tutorial. ACS Meas. Sci. Au 2023, 3 (3), 162–193.
- (38) Giroire, B.; Ali Ahmad, M.; Aubert, G.; Teule-Gay, L.; Michau, D.; Watkins, J. J.; Aymonier, C.; Poulon-Quintin, A. A comparative study of copper thin films deposited using magnetron sputtering and supercritical fluid deposition techniques. *Thin Solid Films* **2017**, *643*, 53–59.
- (39) Singh, G.; Tang, C. R.; Nicoll, A.; Torres, J.; Housel, L. M.; Wang, L.; Takeuchi, K. J.; Takeuchi, E. S.; Marschilok, A. C. Spatiotemporal Resolution of Phase Formation in Thick Porous Sodium Vanadium Oxide (NaV3O8) Electrodes via Operando Energy Dispersive X-ray Diffraction. *J. Phys. Chem. C* **2023**, *127* (8), 3940–3951.
- (40) Tang, C. R.; Singh, G.; Housel, L. M.; Kim, S. J.; Quilty, C. D.; Zhu, Y.; Wang, L.; Takeuchi, K. J.; Takeuchi, E. S.; Marschilok, A. C. Impact of sodium vanadium oxide (NaV 3 O 8, NVO) material synthesis conditions on charge storage mechanism in Zn-ion aqueous batteries. *Phys. Chem. Chem. Phys.* **2021**, 23 (14), 8607–8617.
- (41) Wan, F.; Zhang, L.; Dai, X.; Wang, X.; Niu, Z.; Chen, J. Aqueous rechargeable zinc/sodium vanadate batteries with enhanced performance from simultaneous insertion of dual carriers. *Nat. Commun.* **2018**, *9* (1), 1656–1711.
- (42) Wan, F.; Zhang, L.; Dai, X.; Wang, X.; Niu, Z.; Chen, J. Aqueous rechargeable zinc/sodium vanadate batteries with enhanced performance from simultaneous insertion of dual carriers. *Nat. Commun.* **2018**, 9 (1), 1656.
- (43) Zheng, J.; Zhao, Q.; Liu, X.; Tang, T.; Bock, D. C.; Bruck, A. M.; Tallman, K. R.; Housel, L. M.; Kiss, A. M.; Marschilok, A. C.; et al. Nonplanar Electrode Architectures for Ultrahigh Areal Capacity Batteries. ACS Energy Lett. 2018, 4 (1), 271–275.